

**Carderock Division**  
**Naval Surface Warfare Center**

Bethesda, MD 20084-5000

2  
**AD-A255 431**



**CARDEROCKDIV-SME-92/29 April 1992**

**Ship Materials Engineering Department**  
**Research and Development Report**

**Kink-Band Failure Analysis of Thick Composites**  
**in Compression**

by

E. T. Camponeschi, Jr.<sup>1</sup>

J.W. Gillespie, Jr.<sup>2</sup>

D. J. Wilkins<sup>2</sup>

<sup>1</sup>CARDEROCKDIV, NSWC

<sup>2</sup>Univ. of Delaware, CCM



**92-24645**



4288



Approved for public release, distribution is unlimited.

92 9 0 1 1992

## MAJOR DTRC TECHNICAL COMPONENTS

CODE 011 DIRECTOR OF TECHNOLOGY, PLANS AND ASSESSMENT

12 SHIP SYSTEMS INTEGRATION DEPARTMENT

14 SHIP ELECTROMAGNETIC SIGNATURES DEPARTMENT

15 SHIP HYDROMECHANICS DEPARTMENT

16 AVIATION DEPARTMENT

17 SHIP STRUCTURES AND PROTECTION DEPARTMENT

18 COMPUTATION, MATHEMATICS & LOGISTICS DEPARTMENT

19 SHIP ACOUSTICS DEPARTMENT

27 PROPULSION AND AUXILIARY SYSTEMS DEPARTMENT

28 SHIP MATERIALS ENGINEERING DEPARTMENT

### DTRC ISSUES THREE TYPES OF REPORTS:

1. **DTRC reports, a formal series**, contain information of permanent technical value. They carry a consecutive numerical identification regardless of their classification or the originating department.
2. **Departmental reports, a semiformal series**, contain information of a preliminary, temporary, or proprietary nature or of limited interest or significance. They carry a departmental alphanumeric identification.
3. **Technical memoranda, an informal series**, contain technical documentation of limited use and interest. They are primarily working papers intended for internal use. They carry an identifying number which indicates their type and the numerical code of the originating department. Any distribution outside DTRC must be approved by the head of the originating department on a case-by-case basis.

**Carderock Division**  
**Naval Surface Warfare Center**

Bethesda, MD 20084-5000

---

**CARDEROCKDIV-SME-92/29** April 1992

Ship Materials Engineering Department  
Research and Development Report

**Kink-Band Failure Analysis of Thick Composites  
In Compression**

by  
E. T. Camponeschi, Jr. 1  
J. W. Gillespie, Jr. 2  
D. J. Wilkins 2

1 CARDEROCKDIV, NSWC  
2 Univ. of Delaware, CCM

Accession For	
NTIS CRA&I	<input checked="" type="checkbox"/>
DTIC TAB	<input type="checkbox"/>
Unannounced	<input type="checkbox"/>
Justification	
By	
Distribution/	
Availability Codes	
Dist	Avail and/or Special
A-1	

DTIC QUALITY INSPECTED 1

---

Approved for public release; distribution is unlimited

---

## Table of Contents

List of Tables .....	iv
List of Figures .....	iv
Nomenclature .....	v
Abstract .....	1
Administrative Information .....	1
Introduction .....	1
Theoretical Procedure .....	3
Results and Discussion .....	7
Conclusions .....	11
References .....	12

### **List of Tables**

1. Effective Gage Section Expansion.
2. Theoretical and Experimental Laminate properties Used in Finite Element Analysis
3. Lamina Input Data for Laminate Plate Theory Calculations.
4. Number of Elements and Nodes in Finite Element Model for Each Specimen Thickness.
5. Outer Ply Exit Angle ( $\theta_v$ ) as a Function of Finite Element Mesh Size.
6. Values of  $k$  and  $m$  Used to Determine  $\theta_v$ .
7. Outer Ply Exit Angles.
8.  $\theta_v$  as a function of  $G_{ij}$  nonlinearity (degrees).
9. Laminate Compression Strength and  $0^\circ$  Ply Stress at Failure.
10.  $k_t$  Determined From Compression Failure Theories.

### **List of Figures**

1. Cross Sectional View of the Thick-Section Compression Test Fixture.
2. Representative Kink Band Geometry From a 48 ply 6.4 mm AS4/3501-6 Specimen.
3. Schematic of Effective Gage Section Expansion and Outer Ply Exit Angle.
4. Finite Element Mesh Discretization.
5. Finite Element Model Geometry Used to Determine Outer Ply Exit Angle.
6. Outer Ply Displacement Geometry for AS4/3501-6 Specimens.
7. Theoretical and Experimental Comparison of Compression Strength vs. Thickness For AS4/3501-6.  $k_t$  Determined From 48 Ply Specimens.
8. Theoretical and Experimental Comparison of Compression Strength vs. Thickness For S2 glass/3501-6.  $k_t$  Determined From 48 Ply Specimens.

## Nomenclature

$d$	one-half specimen thickness in the gage section
$E_b$	bolt modulus
$E_1, E_2, E_3$	lamina modulus
$E_x, E_y, E_z$	laminata modulus
$G_{12}, G_{13}, G_{23}$	lamina shear modulus
$G_{xy}, G_{xz}, G_{yz}$	laminata shear modulus
$h$	lamina ply thickness
$k$	coefficient in equation for $\theta_v$
$k_t$	stress concentration factor
$L_b$	bolt length
$m$	exponential coefficient in equation for $\theta_v$
$S_{13}$	is the ultimate transverse shear strength
$t$	specimen thickness within the tabbed section (including tabs)
$t_s$	specimen thickness in the gage section
$w$	element width
$x, y, z$	laminata coordinate directions
$X_1^c$	is the ultimate compression strength
$(X_1^c)_A$	ultimate compression strength, Argon model
$(X_1^c)_R$	ultimate compression strength, Rosen model
$(X_1^c)_B$	ultimate compression strength, Budiansky model
$\alpha_1, \alpha_2, \alpha_3$	lamina coefficients of thermal expansion
$\epsilon_{13}$	ultimate shear strain
$\phi_0$	total misalignment angle ( $\theta_w + \theta_v$ )
$\sigma_c$	longitudinal compressive stress at specimen failure
$\sigma_z$	through-thickness compressive stress due to bolt preload
$\sigma_b$	bolt stress at specimen failure
$\theta_w$	initial misalignment
$\theta_v$	Poisson induced misalignment
$\nu_{12}, \nu_{13}, \nu_{23}$	lamina Poisson's ratios
$\nu_{xy}, \nu_{xz}, \nu_{yz}$	laminata Poisson's ratios

## **Abstract**

*This paper describes an analysis of 6.4 to 25.4 mm (0.25 to 1.0 in.) thick composite laminates subjected to uniaxial compressive loading that experimentally showed a decrease in strength with increasing thickness. The analysis was performed to determine if the reduction in strength was an intrinsic thickness material effect or if it could be attributed to through-thickness restraint on the specimen caused by the test fixture. The analysis was based on closed form solutions for the formation of kink-band failures in the presence of fibers misaligned with the principal axis of compression loading. The fiber misalignment was determined by a finite element analysis that accounted for the displacement of the laminate outer plies where the laminate exited the compression test fixture. The correlation between the experimental results and the theoretical analysis showed the compression strength of the AS4/3501-6 and S2/3501-6 laminates to be independent of thickness and directly proportional to the through-thickness fixture restraint on through-thickness Poisson expansion. This theoretical and experimental comparison also demonstrated a strong correlation between fiber misalignment, its resulting shear stress state and the kink-band compression failure mechanism.*

## **Administrative Information**

This program was supported by the DTRC IR Program Office, sponsored by ONR and administered by Dr. Bruce Douglas, DTRC Code 0113, under work Unit 1-1720-476, and by Mr. Jim Kelly, the Program Area Manager for Materials of the DARPA AST program, under work unit 1-2802-304.

## **Introduction**

Many factors influence the compressive response of composite materials and considered together or separately they can trigger a number of failure modes (1). One factor that has been shown theoretically to have a significant effect on the compression strength of composite materials is fiber misalignment or fiber curvature (2-6). Either of these conditions result in reinforcing fibers that are at an angle to the axis of primary compressive load. Shear stresses can become very high even at small misalignment angles. In addition, carbon and fiberglass reinforced composites exhibit nonlinear shear stress-strain response, resulting in a diminishing shear moduli with increasing shear deformation. Coupled

with the observation that microbuckling based compression failure theories show a strong relationship between shear modulus and compression strength (6, 7), it is understandable that small fiber misalignments could significantly affect compression response by introducing moderate to high shear stresses in the material. Although microbuckling failure is not the only compression failure mechanism possible, and has not been conclusively shown to be the most predominant failure compression mechanism in composites, many investigators have experimentally shown a direct relationship between matrix composite shear modulus and ultimate compression strength (8, 9).

One major weakness of the hypothesis that compression response is strongly influenced by the presence of fiber misalignment and curvature is the lack of experimental data showing direct correlation between actual fiber misalignment or curvature and compression failure initiation. The observation that a fiber misalignment of  $1^\circ$  to  $3^\circ$  from principal load direction significantly reduces compression theoretically, and the assertion that there are fibers misaligned to this degree in every composite compression specimen does not provide substantiation to the subject hypothesis.

In this paper a correlation between experimentally determined compression strength, fiber misalignment angle, and theoretical compression strength is presented. This paper describes the details of the theoretical portion of this correlation with reference to the experimental portion that deals with the compression response of thick (6.4 - 25.4 mm [0.25 - 1.0 in.]) laminates (10). A schematic diagram of the fixture used for the compression testing is shown in Figure 1. A principal objective of the experimental program was to determine the mechanical characteristics of thick composites in compression and observe if they differ from those seen in thinner composite materials. The conclusions drawn from this experimental program are:

- the compressive elastic constants for AS4/3501-6 and S2 glass/3501-6 do not change as specimen thickness increases,
- however, significant through-thickness strains due to nonlinearities in Poisson's ratio developed,

- there was a 20% drop in  $[0_2/90]_{ns}$  compression strength when specimen thickness increased from 6.4 to 25.4 mm (0.25 to 1.0 in.),
- the failure mechanisms did not change with increasing thickness and were predominantly kink band formation and delamination, as seen in thin composite materials,
- compression failures occurred predominantly at the gage-section/tab termination interface.
- in autoclave cured, high quality AS4/3501-6 and S2 glass/3501-6  $[0_2/90]_{ns}$  laminates, through-thickness lamina level waviness along the  $0^\circ$  axis was  $0.660^\circ$  and  $0.820^\circ$  respectively, ref. (11).

Figure 2 shows kink bands at the tab termination region of a 48 ply, 6.4 mm (0.25 in.)  $[0_2/90]_{8s}$  AS4/3501-6 specimen after compression failure.

The fact that the strength of the AS4 and S2 glass laminates decreased 20% even though all other characteristics remained unchanged suggest this phenomenon should be further investigated to determine if it is primarily due to material scaling effects or fixture imposed effects. Since most of the laminate compression failures occurred in the region where the tabs terminated, the effect of experimental technique on failure was theoretically investigated and is presented in this paper. In this region of the specimen, fiber curvature due to the combined effect of gage section Poisson expansion and through-thickness fixture restraint was the largest (Figure 3).

In consideration of the above observations, the objective of the present analysis was to determine if the reduction in compression strength measured in the series of tests on thick coupons could be attributed to the total through-thickness fiber misalignment. Initial fiber waviness was directly measured while misalignment due to fixture restraint was predicted through finite element analysis. This information was then substituted into existing expressions for compression strength modified to include both components of fiber misalignment under consideration and to include stress concentration effects from the fixture induced through-thickness restraint. While the analysis reflects specific conditions defined by the experimental program, this study points out the increasing influence of fixture restraint on inplane compression strength as section thickness increases.

### **Theoretical Procedure**

Since compression strength has been shown theoretically to be strongly influenced by fiber curvature and misalignment, and the value of  $v_{xz}$  measured for the thick laminates is large, the amount of effective thickness expansion (z-direction) in the gage section was examined. The effective through-thickness gage section expansion is defined as the difference between the z-direction expansion that occurs within the gage section of the specimen and that which occurs within the clamped tabbed region of the specimen during the application of a compressive load. The effective gage section expansion is shown schematically in Figure 3. This expansion is of concern since it results in a fiber curvature where the coupon exits the fixture clamping blocks, and is maximum on the specimen outer plies. Figure 3 also shows the angle at which the specimen outer ply exits the clamping blocks as a result of this expansion. If the effective gage section expansion increases with specimen thickness, then so will fiber curvature, resulting in theoretically lower compression strengths for thicker composites.

The three displacement components that influence effective gage section expansion are the free gage section expansion, the specimen contraction under the clamping blocks due to bolt preload, and the specimen and tab expansion within the fixture clamping blocks, and are shown in Figure 3. In order to quantify these effects, the following theoretical approach was applied:

- 1) determine effective gage section expansion using the strength-of-materials bolt analysis and general Hooke's Law for an orthotropic material,
- 2) use this expansion as a uniform displacement boundary condition in a finite element analysis to determine outer ply displacement geometry,
- 3) determine the effect of fiber misalignment on compression strength using a compression failure theory that is based on a kink band failure mechanism.

In addition to this approach, a finite element model of 1/4 of the complete fixture-specimen assembly with uniform end loading was also performed. The gage section expansion determined using this approach was the same as that determined in step 1) above. Since a large number of elements were needed for the convergence study performed, the strength-of-materials solution for gage section expansion was utilized and only a portion of the specimen/tab for each laminate thickness region was analyzed using the finite element procedure.

The free gage section expansion can be expressed as:

$$\frac{\sigma_c t_s \nu_{xz}}{E_x} \quad 1$$

where

$\sigma_c$  = longitudinal compressive stress at specimen failure

$t_s$  = specimen thickness in the gage section

$\nu_{xz}$  = through-thickness Poisson's ratio

$E_x$  = longitudinal modulus

Preload contraction can be expressed as:

$$\frac{\sigma_z t}{E_z} \quad 2$$

where

$\sigma_z$  = through-thickness compressive stress due to bolt preload

$t$  = specimen thickness within the tabbed section (including tabs)

$E_z$  = through thickness modulus

and the specimen and tab expansion within the fixture clamping blocks due to the applied longitudinal compressive stress as:

$$\frac{\sigma_b L_b}{E_b}$$

3

where

$\sigma_b$  = bolt stress at specimen failure, reference (12)

$L_b$  = bolt length

$E_b$  = bolt modulus

Finally the effective gage section expansion,  $\Delta_{eff}$  can be expressed as:

$$\Delta_{eff} = \frac{\sigma_c t_s v_{xz}}{E_x} + \frac{\sigma_z t}{E_z} - \frac{\sigma_b L_b}{E_b}$$

4

The finite element code used to determine the outer ply displacement geometry resulting from the gage section expansion was ABAQUS developed by HKS, and was run on a Digital Equipment Corp. MicroVax. A 2-D analysis using 2nd order plane-strain orthotropic elements for the composite specimen and tabs was performed.

From the finite element modeling the outer ply displacement and exit angle (shown in Figure 3) were determined. This information was then used as input into failure theories that are based on kink band formation as the principal mechanism of failure for fiber-reinforced composite materials.

Argon (2) and Budiansky (3) have both proposed compression failure theories that were developed based on the observation of kink band formation in compressively loaded orthotropic materials. They also include a fiber misalignment angle term in their analysis as the geometric perturbation that creates a region of increased shear stress and triggers failure due to instability.

In the work by Argon, he considers a region of initial misalignment ( $\phi_0$ ) with respect to the loading axis in a fiber reinforced composite. This region causes an interlaminar shear stress and a corresponding element rotation, that further increases shear stress until shear collapse instability occurs. This model parallels an analysis of the formation of kink bands in metal crystals. His derivation leads to an expression for the compression strength of

$$(X_1^c)_A = \frac{S_{13}}{\phi_o} \quad 5$$

where  $X_1^c$  is the compression strength,  $S_{13}$  is the ultimate transverse shear strength, and  $\phi_o$  is the initial misalignment angle.

Budiansky extended Rosen's (7) elastic shear microbuckling solution for the ultimate compression strength  $X_1^c$

$$(X_1^c)_R = G_{13} \quad 6$$

to include plasticity, assuming perfect plasticity in shear beyond  $\gamma = \epsilon_{13} = S_{13}/G_{13}$  and fiber misalignment. The resulting expression is

$$(X_1^c)_B = \left[ \frac{\epsilon_{13}}{\phi_o + \epsilon_{13}} \right] (X_1^c)_R = \left[ \frac{\epsilon_{13}}{\phi_o + \epsilon_{13}} \right] G_{13} \quad 7$$

The analyses by both Argon and Budiansky assume the presence of an initial fiber misalignment. In applying these analyses to the thick compression specimens tested in this program, fixture induced fiber misalignment that occurs with the application of a compressive load is considered equally as important as the initial misalignment. Therefore the term  $\phi_o$  in eqs. 5 and 7 is generalized to include both initial misalignment ( $\theta_w$  since in this study lamina waviness creates the misalignment) and Poisson induced misalignment  $\theta_v$ . In the present analysis the magnitude of  $\sigma_1$  in the  $0^\circ$  plies of the  $[0_2/90]_{ns}$  laminate is determined from classical lamination theory.

These analyses also do not include the effects of transverse inplane and through-thickness normal stresses. For the  $[0_2/90]_{ns}$  laminates in this study inplane transverse normal stresses are present from transverse ply restraint and through-thickness normal stress from fixture restraint. Inplane normal stresses are neglected, and through-thickness normal stress contributions are accounted for with the addition of a stress concentration term on the longitudinal lamina stress that is determined

from laminate plate theory and far field laminate stress. The resulting expressions for compression strength are:

$$k_t(X_1^c)_A = \frac{S_{13}}{(\theta_w + \theta_v)} \quad (8)$$

$$k_t(X_1^c)_B = \left[ \frac{\epsilon_{13}}{(\theta_w + \theta_v) + \epsilon_{13}} \right] G_{13} \quad (9)$$

This stress concentration factor was defined through a correlation between the experimental results at a single specimen thickness (6.4 mm) and the finite element stress analysis for this thickness. Consequently eqs. 8 and 9 are not newly derived expressions for compression strength, but rather are variations of the original solutions by Argon and Budiansky to account for observations from the experimental thick-section compression test results.

### Results and Discussion

The effective gage section expansion determined by equation 4 is a linear function of specimen thickness. The contributions from each term in equation 4 along with the effective gage section expansion are listed in Table 1 for each material and thickness.

The laminate material properties used in the finite element analyses and the effective gage section expansion calculations are the values from Table 2. The theoretical values were determined using experimentally determined lamina properties (Table 3) and Pagano's exact theory for determining 3D orthotropic laminate properties (13, 14). The details of the theoretical procedure are included in ref. (12). The values for laminate shear moduli are initial tangent moduli values, however preliminary finite element analyses with shear moduli decreased 40% showed a 20% increase in outer ply exit angle. Therefore the shear moduli used in the ABAQUS finite element runs were 60% of those in Table 2. A value of 60% was chosen since this moduli is equal to the secant modulus defined from 0 strain up to the point where the curve flattens out for the two materials tested by the ASTM D3518 method. Data documenting the specific effect of reduced shear moduli on outer ply exit angle will follow.

In order to provide the outer ply exit angle needed for the models by Argon and Budiansky, the finite element modeling scheme shown in Figures 4 and 5 was used. These figures show the finite element mesh discretization used for the coarsest mesh studied and the application of a constant displacement boundary condition, respectively. The magnitude of the through-thickness displacement to be applied was determined by taking one half of the effective expansion in Table 2 and multiplying it by the ratio of the free gage section thickness plus tab thickness to the free gage section thickness. 2nd order, plane strain elements with an aspect ratio of 2:1 were used for the analysis. Although the figures in this paper show a line of distinction between the tabs and the specimen, the tabs used in the experimental study were made of the same material and stacking sequence as the specimens so all analyses assumed continuous material properties across the tab-specimen boundary.

Figure 6 shows preliminary results for the outer ply displacement geometry for the all three thicknesses of the AS4/3501-6 specimens, and shows an increase in the outer ply exit angle with increasing specimen thickness. After these preliminary results, a mesh refinement study beginning with the mesh discretization shown in Figure 5 was conducted. Analyses with mesh refinement to 1/16 the size shown in Figure 5 were conducted to determine solution convergence. The number of elements and corresponding number of nodes used in the convergence study is summarized in Table 4.

Table 5 lists the values of  $\theta_v$  determined for each material and specimen thickness and for each mesh size analyzed. A mathematical analysis of this data indicates  $\theta_v$  does not converge with decreasing mesh size (12). Consequently, an average exit angle is defined consistent with the mesh discretization and the heterogeneity of the laminated system (ie. a repeating sublaminate). A convergent exponential form for  $\theta_v$  as a function of  $z$  was formulated. This form is

$$\theta_v = kz^m \quad (10)$$

The coefficients of this equation were determined from a plot of  $\ln(\theta_n)$  versus  $\ln(z)$ . The values for  $k$  and  $m$  are listed in Table 6. Integrating equation 10 will yield

$$\theta_{v-ave} = \frac{k}{-m + 1} l^{-m} \quad (11)$$

which is an average value of  $\theta_v$  over a specified distance  $l$ .

The  $\theta_v$  data to be used in the averaging procedure was taken from the ABAQUS runs with an x-direction element size of 0.2 mm (0.0078 in.) The values for the outer ply exit angles calculated using  $k$  and  $m$  from Table 6 and equation 11 are listed in Table 7. The dimension ( $l$ ) over which the values of  $\theta_v$  were determined was 0.38 mm (0.015 in.) This dimension is equivalent to three ply thicknesses, and equals the dimension of the repeating  $[0_2/90]$  sublaminate used in the thick laminates tested. This table also lists the average lamina level waviness measured for the  $[0_2/90]_{ns}$  laminates, and the total fiber misalignment angle resulting from a superposition of the initial misalignment and the misalignment at failure due to fixturing effects.

As previously mentioned, the shear moduli used in the calculation of the outer ply exit angles in Table 7 were 60% of those listed in Table 2. These values were used since  $\theta_v$  was found to be sensitive to the laminate shear moduli. This sensitivity was quantified using the averaging technique for 0.38 mm (0.015 in.) of the laminate thickness as described above for the calculation of the outer ply exit angle with laminate thickness. The effect of shear moduli nonlinearity are shown in Table 8, and the results show a 25% increase in outer ply exit angle with a 40% drop in shear moduli. The actual effect of shear nonlinearity may be greater than shown here, since only a linear analysis was performed, and the instantaneous shear moduli that could be used in a nonlinear analysis would be much less than the secant moduli used here. A nonlinear analysis could be performed by exercising the UMAT option in ABAQUS that allows for nonlinear material properties through user written material property subroutines. Although not used for this program, this option is being investigated in related Navy programs.

Considering equations 8 and 9,  $(\theta_w + \theta_v)$  is now known and  $X_x^c$  has been determined experimentally. The laminate strength for each specimen thickness are listed in Table 9. Since the stress at failure in the outer  $0^\circ$

plies is necessary for these equations, the  $0^\circ$  ply  $X_1^C$  (Table 9) was determined using classical lamination theory and the lamina properties from Table 3, including residual thermal stresses for a  $\Delta T$  of  $138^\circ\text{C}$ .

$S_{13}$  and  $\epsilon_{13}$  are also required to evaluate  $k_t$  from equations 8 and 9. From the  $[\pm 45]$  tension tests run to determine  $G_{13}$  in Table 3,  $S_{13}$  was found to be 75.8 MPa (11,000 psi) for both the AS4/3501-6 and the S2 glass/3501-6 materials. Coupon failure did not occur at 75.8 MPa (11,000 psi) for these materials, but the shear stress-strain curve flattened out at this stress. To be consistent with Budiansky's (7) assumption of elastic perfectly plastic shear response beyond a given shear strain, the values of  $G_{13}$  reduced 40% and  $S_{13}$  of 75.8 MPa (11,000 psi) were used to calculate  $\epsilon_{13}$ . The resulting values were 2.1% for AS4/3501-6 and 1.9% for S2 glass/3501-6.

Substituting  $0^\circ$  ply  $X_1^C$ ,  $(\theta_w + \theta_v)$ , and  $S_{13}$  or  $\epsilon_{13}$  into equation 8 and 9 provides the stress concentration factor for each laminate. These values are listed in Table 10, and are seen to be comparable for each laminate thickness, although they differ depending on which compression failure theory was used (see eq. 8 and 9). The fact that  $k_t$  is unchanged with thickness suggests that the strength of these laminates should not change with thickness and to further investigate this observation, the values of  $k_t$  from the 48 ply specimens were used to predict the strength of the 96 and 192 ply laminates considering the fiber exit angle determined for each of these thicknesses. These results are shown in Figures 7 and 8 and show a decreasing trend in theoretical compression strength of the same magnitude as the experimentally measured values. These figures also show that the consideration of initial waviness alone will not change compression strength with increasing specimen thickness.

It should be noted here that the stress concentration factors and the distance over which integration was performed to determine  $q_n$  cannot be applied in general to the compressive failure of composite materials. Instead these terms have been used within in a consistent theoretical framework to determine the effect of a specific fixture geometry on compression coupons of increasing thickness. For variations of fixture and specimen geometry a comparable set of experiments with associated analysis should be performed to determine these factors. Within the scope of this discussion, the above analysis has been used to show that a shear

based failure in compression specimens has occurred in the region of high fiber misalignment, and is related to the shear stress caused by fiber misalignment. This correlation between theoretical predictions and experimental observations is otherwise difficult to make due to the sensitivity of compression response to the many local inhomogeneities that may be present.

When considering the use of thick composites in structural applications, the effect of through-thickness Poisson expansion must be closely considered in areas where through-thickness restraint is present. Through-thickness restraint by test fixtures is beneficial in preventing premature end failures in end-loaded compression coupons, however the effect of this restraint near the gage region has been shown to be undesirable in this study, and worsens as specimen thickness increases. In addition to the compression test methods analyzed in this program, this method of accounting for the effect of through-thickness displacements on compression strength should be extended to structural details such as joints. As with compression tests specimens, the tradeoffs between desired effects of restraint (prevention of end initiated failures or failure due to high through-thickness stresses) and undesirable effects must be balanced.

### **Conclusions**

This paper describes an analysis performed on thick composite specimens tested to failure in compression. The results have shown that there is no inherent effect of thickness on the strength of carbon and S2 glass reinforced laminates even though a drop in strength was observed experimentally. Decreases in compression strength observed for specimens from 6.4 to 25.4 mm have been shown to be caused by through-thickness fixture induced effects. The fixture restraint on through-thickness Poisson expansion results in through-thickness fiber misalignment that is significant enough to account for the reduction in measured compression strength.

This and other results from this investigation suggest that what has been learned from the evaluation and analysis of thin composites in compression can be used in the evaluation and analysis thick composites in compression. And conversely, what has been learned from experiments and analysis of thick composites can be used to further guide the

development of failure theories for composite materials in more conventional thicknesses. In particular, the correlation of experimental results with results predicted by kink band based failure theories suggest continued work in this area. Current failure theories that are based on the kink-band failure mechanism are very simplistic and could benefit from further development . The inclusion of nonlinear shear stress strain response in these theories is an area in need of development.

A correlation between fiber misalignment angle and compression strength was shown both experimentally and theoretically in this work. Little information exists on the magnitude and dispersion of misalignment in typical fiber reinforced composites and this area should be further investigated. Data documenting the amplitude and wavelength of fiber waviness is almost nonexistent and is needed for further understanding of this effect on compression strength.

Finally, with the interest in using composite materials for larger and thicker structures the need to account for Poisson induced fiber misalignment as documented in this study becomes important. In many joint concepts that could be envisioned for thick composite structures, a through-thickness restraint is present, and the effect of this restraint must be considered when the material is subjected to inplane compressive stress.

## References

1. Camponeschi, E. T., Jr., "Compression of Composite Materials: A Review", *Fatigue and Fracture of Composite Materials (Third Conference)*, ASTM STP 1110, T.K. O'Brien, Ed., ASTM, 1991, pp. 550-580.
2. Argon, A. S., "Fracture of Composites," *Treatise on Materials Science and Technology*, 1972, 1:pp. 106-114.
3. Budiansky, B., "Micromechanics," *Computers and Structures*, 1983, 16(1-4):pp. 6-10.
4. Davis, J. G., Jr., "Compressive Strength of Fiber-Reinforced Composite Materials", *Composite Reliability*, ASTM STP 580, ASTM, 1975, pp. 364-377.
5. Wang, A. S. D., "Non-Linear Microbuckling Model Predicting the Compressive Strength of Unidirectional Composites," ASME Rep. No. Paper 78-WA/Aero-1, 1978.
6. Shuart, M. J., "Short-Wavelength Buckling and Shear Failures for Compression-Loaded Composite Laminates," NASA Rep. No. TM-87640, Nov., 1985.
7. Rosen, B. W., "Mechanics of Composite Strengthening", *Fiber Composite Materials*, ASM, 1964.
8. Sohi, M. M., Hahn, H. T., and Williams, J. G., "The Effect of Resin Toughness and Modulus on Compression Failure Modes of Quasi-Isotropic Graphite/Epoxy Laminates", *Toughened Composites*, ASTM STP 937, Johnston, Ed., ASTM, 1987, pp. 37-60.
9. Yurgartis, S. W., "The Influence of Matrix Properties and Composite Microstructure on the Longitudinal Compression Strength of High-Performance Composites," Ph. D. Dissertation, Rensselaer Polytechnic Institute, Troy, New York, Dec., 1987.
10. Camponeschi, E. T., Jr., "Compression Testing of Thick-Section Composite Materials", *Fatigue and Fracture of Composite Materials (Third Conference)*, ASTM STP 1110, T.K. O'Brien, Ed., ASTM, 1991, pp. 439-456.
11. Camponeschi, E. T., Jr., "Lamina Waviness Levels in Thick Composites and its Effect on Their Compression Strength," *Proceedings of ICCM 8*, 1991, Tsai and Springer, SAMPE.

12. Camponeschi, E. T., Jr., "Compression Response of Thick-Section Composite Materials," Ph.D Dissertation, Univ. of Delaware, August, 1990.
13. Pagano, N. J., "Exact Moduli of Anisotropic Laminates", *Mechanics of Composite Materials*, Sendekyj, Ed., Academic Press, 1984, pp. 23-44.
14. Trethewey, B. R., Jr., Wilkins, D. J., and Gillespie, J. W., Jr., "Three-Dimensional Elastic Properties of Laminated Composites," Univ. of DE Rep. No. CCM Report 89-04, 1989.
15. Knight, M., "Three-Dimensional Elastic Moduli of Graphite/Epoxy Composites," *Journal of Composite Materials*, Vol. 16, 1982, pp. 153-159.

Table 1 Effective Gage Section Expansion.

	Eq. 1 Free Expansion mm (in.)	Eq. 2 Preload Contraction mm (in.)	Eq. 3 Restrained Expansion mm (in.)	Eq. 4 Effective Expansion mm (in.)
AS4/3501-6				
48 ply	0.0483 (0.0019)	0.0076 (0.0003)	0.0254 (0.0010)	0.0305 (0.0012)
96 ply	0.0838 (0.0033)	0.0178 (0.0007)	0.0508 (0.0020)	0.0508 (0.0020)
192 ply	0.1524 (0.0060)	0.0330 (0.0013)	0.0965 (0.0038)	0.0889 (0.0035)
S2/3501-6				
48 ply	0.0787 (0.0031)	0.0025 (0.0001)	0.0559 (0.0022)	0.0253 (0.0010)
96 ply	0.1372 (0.0054)	0.0076 (0.0003)	0.1041 (0.0041)	0.0407 (0.0016)
192 ply	0.2540 (0.0100)	0.0178 (0.0007)	0.1981 (0.0078)	0.0737 (0.0029)

**Table 2 Theoretical and Experimental Laminate properties Used in Finite Element Analysis**

	AS4/3501-6 [0 <sub>2</sub> /90] <sub>ns</sub>		S2 glass/3501-6 [0 <sub>2</sub> /90] <sub>ns</sub>	
	Theor.	Exp.	Theor.	Exp.
E <sub>x</sub> GPa (Msi)		71.8 (10.41) [3.7] <sup>1</sup> [26] <sup>2</sup>		38.0 (5.51) [7.2] [31]
E <sub>y</sub> GPa (Msi)	41.9 (6.08)		22.9 (3.32)	
E <sub>z</sub> GPa (Msi)	13.1 (1.90)		13.4 (1.95)	
ν <sub>xy</sub>		0.072 [7.3] [5]		0.156 [4.6] [7]
ν <sub>xz</sub>		0.508 [3.6] [14]		0.450 [5.7] [14]
ν <sub>yz</sub>	0.613		0.617	
G <sub>xy</sub> GPa (Msi)	6.00 (0.87)		6.76 (0.98)	
G <sub>xz</sub> GPa (Msi)	5.03 (0.73)		5.38 (0.78)	
G <sub>yz</sub> GPa (Msi)	4.34 (0.63)		4.41 (0.64)	

1 coefficient of variation

2 number of data points in average

Table 3 Lamina Input Data for Laminate Plate Theory Calculations.

	AS4/3501-6	S2 glass/3501-6
$E_1$ GPa (Msi)	107.1 (15.54) [3.5] <sup>1</sup>	48.6 (7.05) [4.7]
$E_2$ GPa (Msi)	8.83 (1.28) [3.9]	9.72 (1.41) [3.5]
$E_3$ GPa (Msi)	8.83 (1.28) <sup>2</sup>	9.72 (1.41)
$\nu_{12}$	0.352 [1.2]	0.311 [5.0]
$\nu_{13}$	0.350 [2.1]	0.331 [5.7]
$\nu_{23}$	0.649 [2.0]	0.690 [3.4]
$G_{12}$ GPa (Msi)	6.00 (0.87) <sup>3</sup>	6.76 (0.98)
$G_{13}$ GPa (Msi)	6.00 (0.87) <sup>4</sup>	6.76 (0.98)
$G_{23}$ GPa (Msi)	3.79 (0.55) <sup>5</sup>	3.79 (0.55)
$\alpha_1$ m/m/°C	$-1.4 \times 10^{-7}$	$1.3 \times 10^{-6}$
$\alpha_2$ m/m/°C	$0.8 \times 10^{-5}$	$1.1 \times 10^{-6}$
$\alpha_3$ m/m/°C	$0.8 \times 10^{-5}$	$1.1 \times 10^{-6}$

1 coefficient of variation (%)

2  $E_3$  assumed equal to  $E_2$

3  $G_{12}$  determined from  $[\pm 45]_{2s}$   
tension test

4  $G_{13}$  assumed equal to  $G_{12}$

5  $G_{23}$  from reference (15)

**Table 4 Number of Elements and Nodes in Finite Element Model for Each Specimen Thickness.**

Element width, mm, (in.)	48 ply Specimens		96 ply Specimens		192 ply Specimens	
	elements	nodes	elements	nodes	elements	nodes
0.7950 (0.0313)	24	97	80	285	320	1049
0.3962 (0.0156)	96	337	320	1049	1280	4019
0.1981 (0.0078)	384	1249	1280	4019	5120	15713
0.0991 (0.0039)	1536	4811	5120	15713	---	---
0.0660 (0.0026)	3456	10657	---	---	---	---

Table 5 Outer Ply Exit Angle ( $\theta_v$ ) as a Function of Finite Element Mesh Size.

$\theta_v$ (degrees) Values for AS4/3501-6 Specimens					
	Element Width, mm (in.)				
	0.7950 (0.0313)	0.3962 (0.0156)	0.1981 (0.0078)	0.0991 (0.0039)	0.0660 (0.0026)
48 ply	0.648	0.885	1.17	1.52	1.76
96 ply	0.796	1.06	1.37	1.77	---
192 ply	0.914	1.19	1.54	---	---

$\theta_v$ (degrees) Values for S2 glass/3501-6 Specimens					
	Element Width, mm (in.)				
	0.7950 (0.0313)	0.3962 (0.0156)	0.1981 (0.0078)	0.0991 (0.0039)	0.0660 (0.0026)
48 ply	0.560	0.768	1.02	1.33	---
96 ply	0.662	0.880	1.15	1.49	---
192 ply	0.807	1.105	1.36	---	---

Table 6 Values of k and m Used to Determine  $\theta_v$ .

Values of k and m Used to Determine $\theta_v$				
	AS4/3501-6		S2 glass/3501-6	
	k	m	k	m
48 ply	0.00173	0.38	0.00151	0.38
96 ply	0.00219	0.38	0.00185	0.38
192 ply	0.00258	0.38	0.00230	0.38

Table 7 Outer Ply Exit Angles.

	$[0_2/90]_{8s}$	$[0_2/90]_{16s}$	$[0_2/90]_{32s}$
AS4/3501-6			
Expansion $\theta_v$ , (°)	0.789	0.998	1.18
Initial $\theta_w$ , (°)	0.660	0.660	0.660
Total $\phi_o$ , (°)	1.45	1.66	1.84
(radians)	(0.0253)	(0.0289)	(0.0321)
S2 glass/3501-6			
Expansion $\theta_v$ , (°)	0.688	0.843	1.05
Initial $\theta_w$ , (°)	0.820	0.820	0.820
Total $\phi_o$ , (°)	1.51	1.66	1.87
(radians)	(0.0263)	(0.0290)	(0.0326)

Table 8  $\theta_v$  as a function of  $G_{ij}$  nonlinearity (degrees).

$\theta_v$ as a function of $G_{ij}$ nonlinearity (degrees)		
	AS4/3501-6	S2/3501-6
$G_{ij}$	0.658	0.579
(0.8) $G_{ij}$	0.728	0.637
( $\Delta$ )	(10.6%)	(10.0%)
(0.6) $G_{ij}$	0.829	0.728
( $\Delta$ )	(26.0%)	(25.7%)

Table 9 Laminate Compression Strength and 0° Ply Stress at Failure.

	$[0_2/90]_{8s}$	$[0_2/90]_{16s}$	$[0_2/90]_{32s}$
AS4/3501-6			
Laminate $X_x^c$ GPa (ksi)	1.074 (155.9)	0.891 (129.3)	0.841 (122.1)
0° Ply $X_1^c$ GPa (ksi)	1.565 (227.0)	1.302 (188.8)	1.230 (178.4)
S2 glass/3501-6			
Laminate $X_x^c$ GPa (ksi)	0.989 (143.4)	0.930 (134.9)	0.798 (115.7)
0° Ply $X_1^c$ GPa (ksi)	1.370 (198.7)	1.289 (187.0)	1.109 (160.8)

Table 10  $k_t$  Determined From Compression Failure Theories.

	$[0_2/90]_{8s}$	$[0_2/90]_{16s}$	$[0_2/90]_{32s}$	Average
$k_t$ Argon				
AS4/3501-6	1.92	2.01	1.92	1.95
S2 glass/3501-6	2.10	2.03	2.10	2.08
$k_t$ Budiansky				
AS4/3501-6	1.04	1.16	1.15	1.12
S2 glass/3501-6	1.25	1.25	1.35	1.28

## THICK-SECTION COMPRESSION TEST METHOD

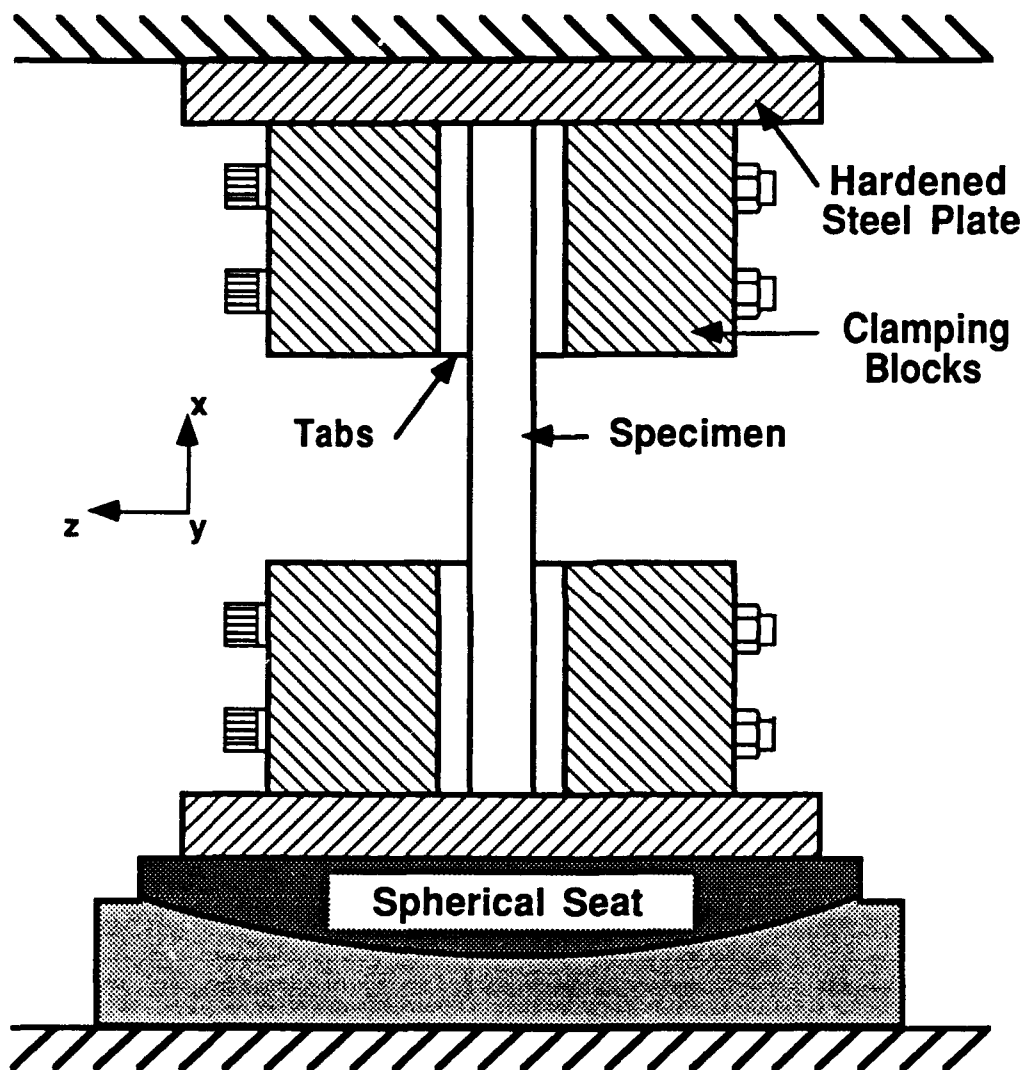


Figure 1 Cross Sectional View of the Thick-Section Compression Test Fixture.

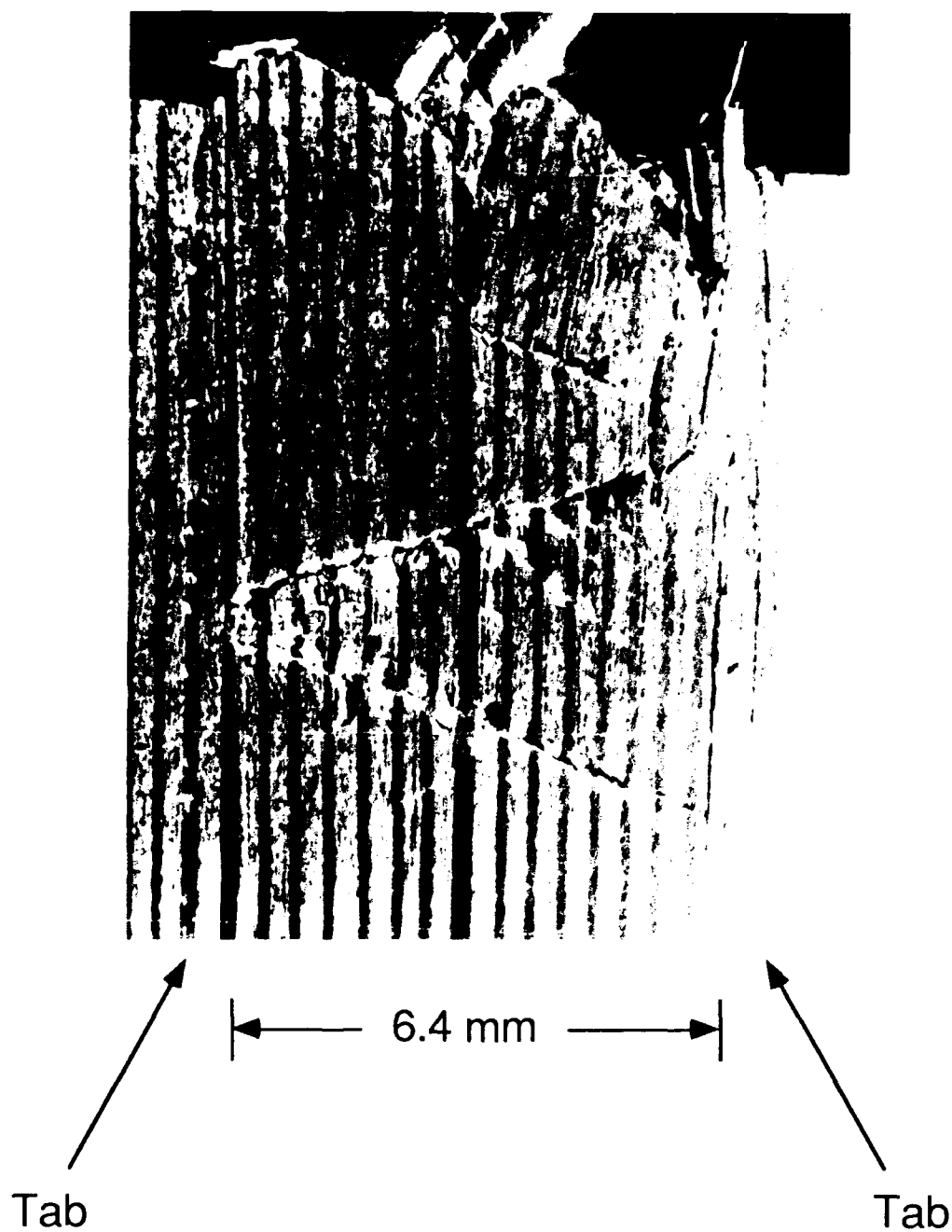


Figure 2 Representative Kink Band Geometry From a 48 ply 6.4 mm AS4/3501-6 Specimen.

## Effective Gage Section Expansion and Outer Ply Exit Angle

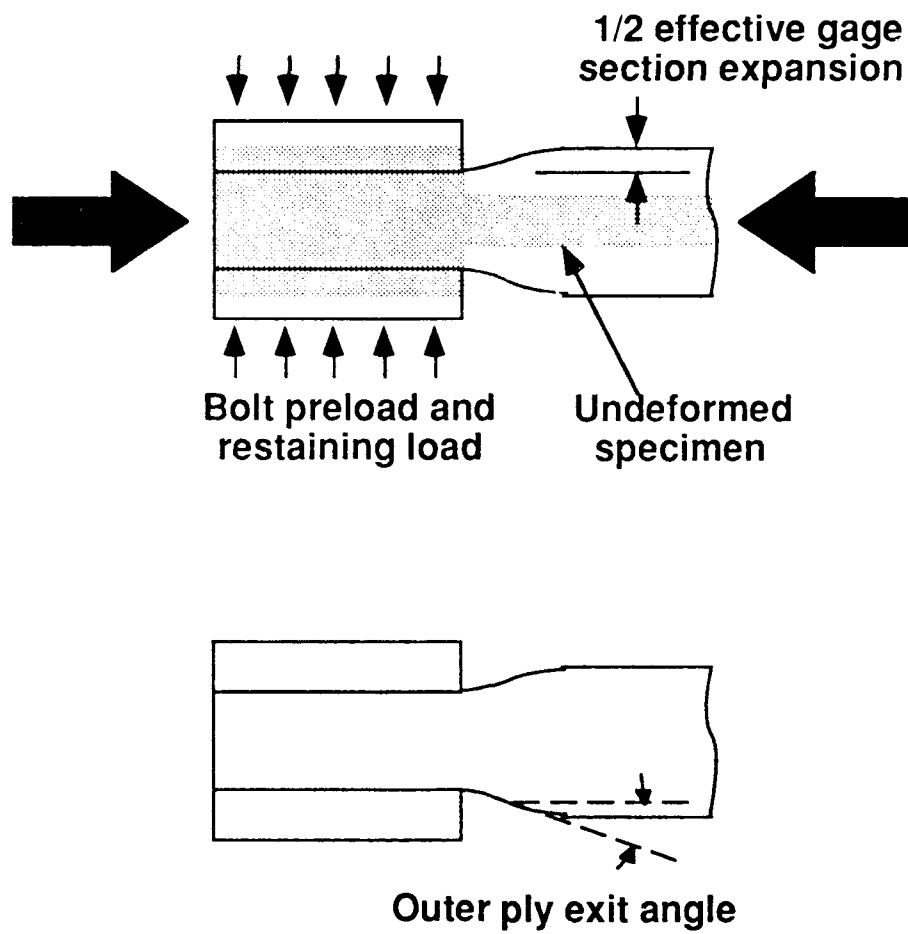


Figure 3 Schematic of Effective Gage Section Expansion and Outer Ply Exit Angle.

## Finite Element Mesh Discretization

Coarsest Mesh (element width,  $w = 0.795 \text{ mm}$  [0.0313 in.])

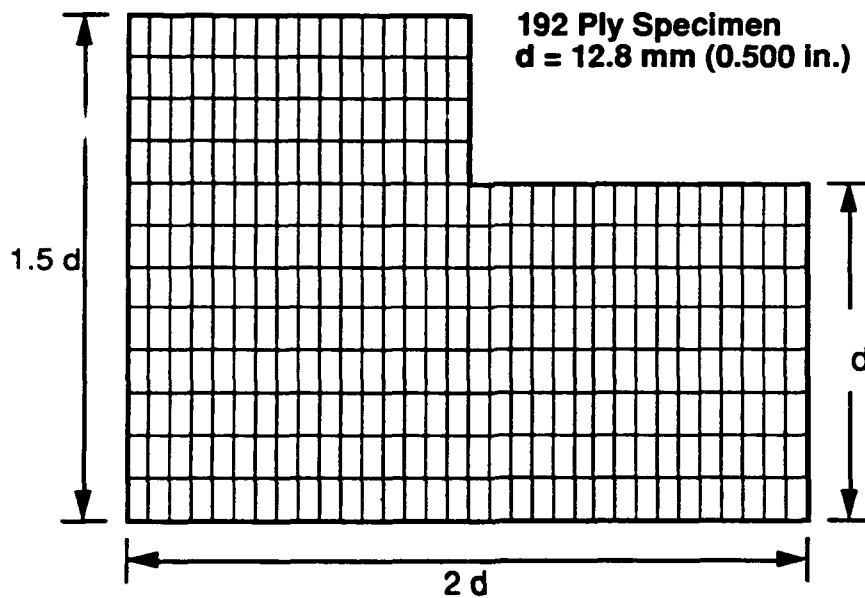
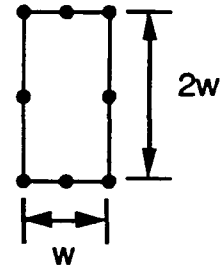
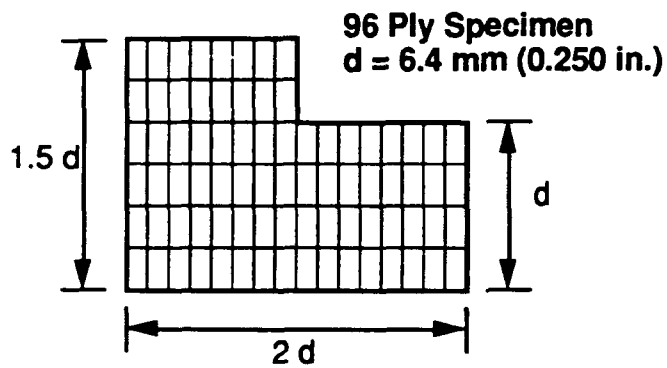
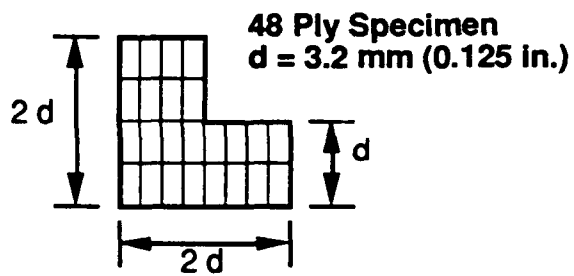


Figure 4 Finite Element Mesh Discretization

Uniform Displacement  
Boundary Condition

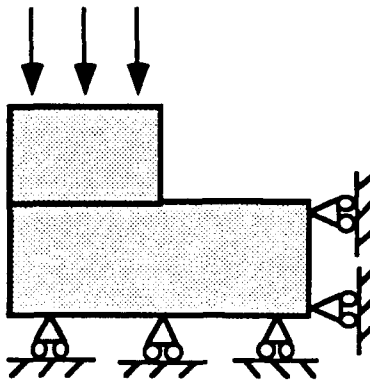


Figure 5 Finite Element Model Geometry Used to Determine Outer Ply Exit Angle.

### Through-Thickness Displacement for [0/0/90] Carbon/Epoxy Laminates

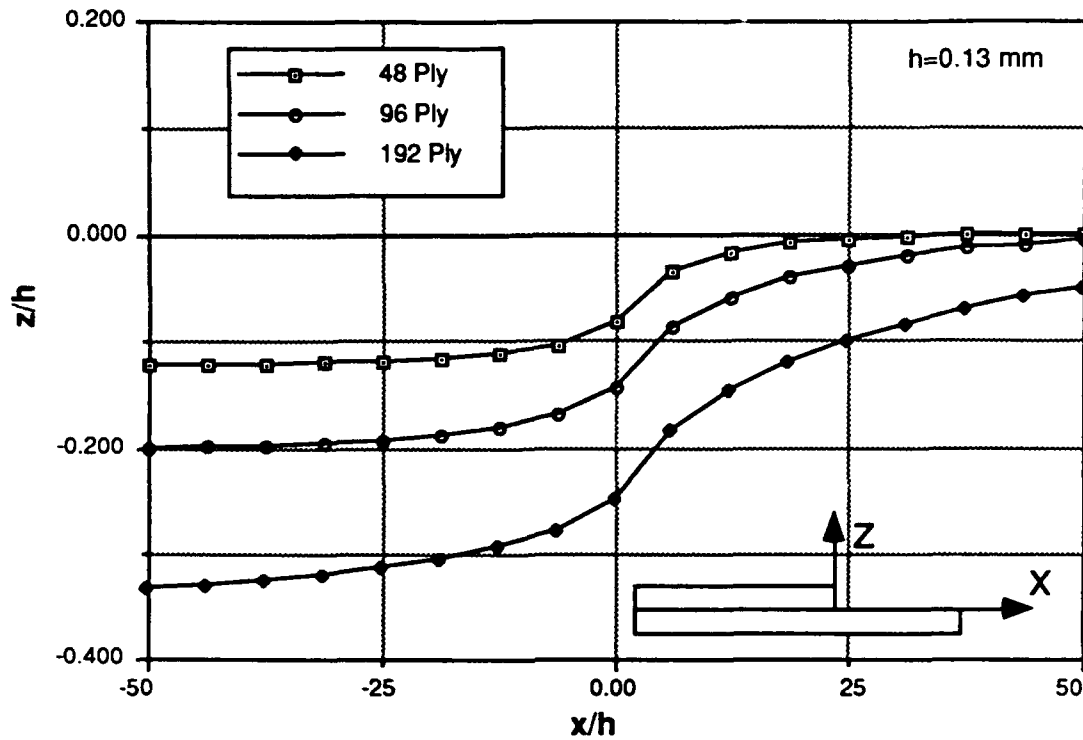


Figure 6 Outer Ply Displacement Geometry for AS4/3501-6 Specimens.

**Compression Strength Considering  
Fiber Misalignment at Failure Stress  
[0/0/90] AS4/3501-6 Laminates**

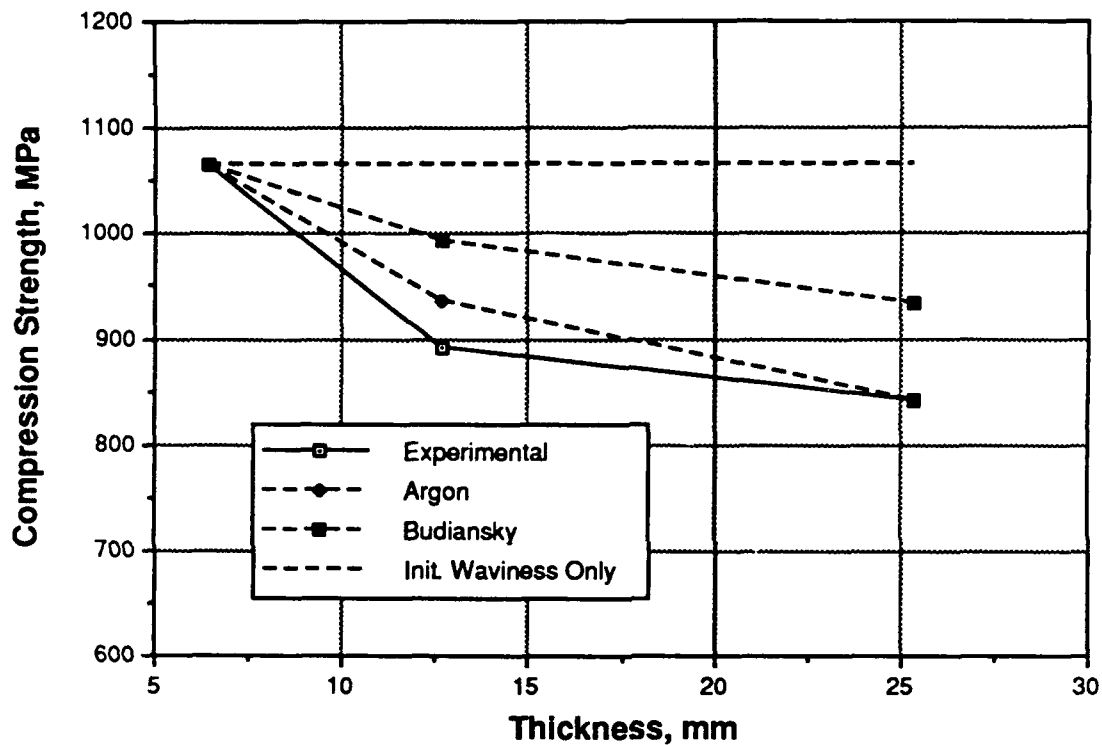


Figure 7 Theoretical and Experimental Comparison of Compression Strength vs. Thickness For AS4/3501-6.  $k_t$  Determined From 48 Ply Specimens.

**Compression Strength Considering  
Fiber Misalignment at Failure Stress  
[0/0/90] S2 Glass/3501-6 Laminates**

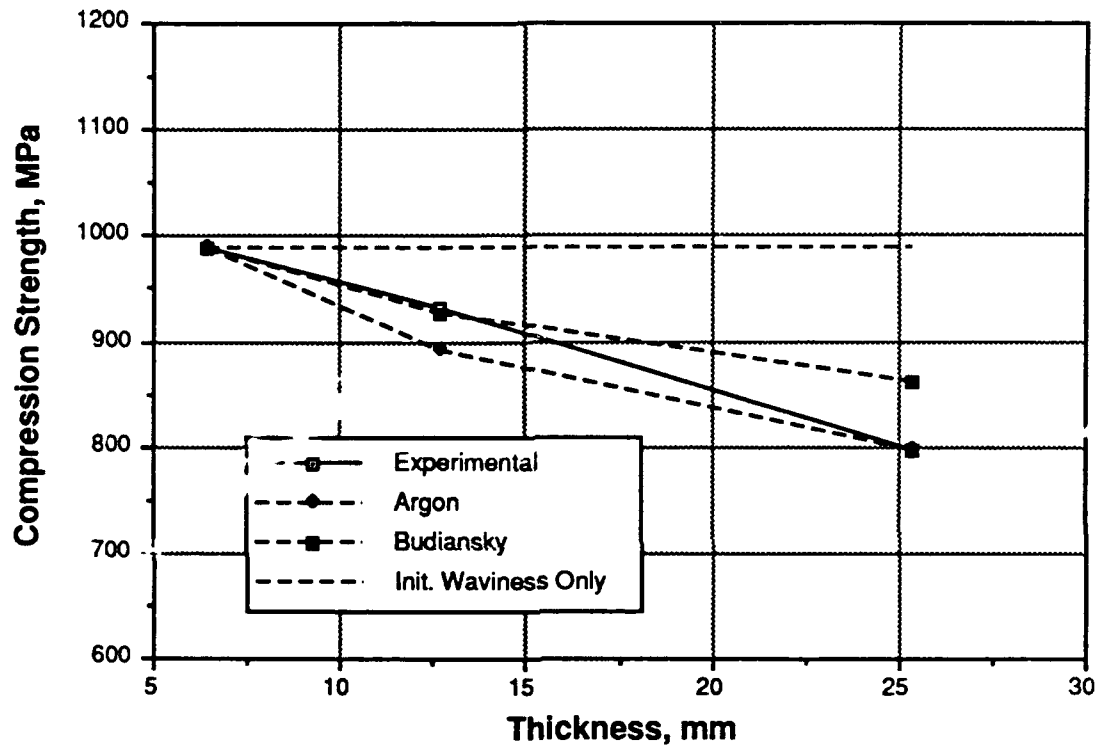


Figure 8 Theoretical and Experimental Comparison of Compression Strength vs. Thickness For S2 glass/3501-6.  $k_t$  Determined From 48 Ply Specimens.

# INITIAL DISTRIBUTION

Copies	CENTER DISTRIBUTION		
	Copies	Code	Name
12 DTIC	1	0115	Caplan
1 DARPA	1	0112	Douglas
1 (Kelly)	1	17	Krenzke
	1	1702	Corrado
1 COMNAV Spec. War Com.	1	172	Rockwell
San Diego CA 92155	1	176	Sykes
1 006 (Walker)	3	1720.2	Phyllaier
7 NAVSEA	1	1720.4	Wiggs
1 05M3 (Pinto)	1	1730.2	Critchfield
1 92R (Troffer)	1	2723	Wilhelmi
1 92R (Spero)	1	274	Wang
1 55Y2 (McCarthy)	1	28	Wacker
1 55Y2 (Will)	5	2802	Morton
1 55Y2 (Nichols)	5	2802	Camponeschi
1 PMS 395 (Nyers)	1	2803	Cavallaro
3 NRL	1	284	Fischer
1 6383 (Badaliance)	1	2844	Castelli
1 6383 (Wolock)	1	522.2	TIC (A)
1 6385 (Chaskelis)	1	522.1	TIC (C)
1 NSWC	1	5231	Office Services
1 R31 (Augl)			
4 ONR			
1 1132SM (Rajapakse)			
1 1131S (Fishman)			
1 1132SM (Barsoum)			
1 1216 (Vasudevan)			
1 ONT			
1 233 (Remmers)			

INITIAL DISTRIBUTION (Continued)

2

IDA S&T Division  
1801 N. Beauregard St.  
Alexandria, VA, 22311  
Attn. Mr. Charles Bersch  
Attn. Mr. George Sorkin

Dr. R.E. Bohlmann  
McDonnell Aircraft Company  
Dept. 337, Bldg. 102 MC1021310  
James S. McDonnell Blvd.  
Berkely, MO 63134

Dr. Francis Chang  
GD/Fort Worth Div, MZ 5984  
PO Box 748  
Fort Worth, TX 76101

Mr. Brian Coffenberry  
ICI Composite Structures  
2055 East Technology Circle  
Tempe, AZ 85284

Mr. Richard Collins  
Grumman Aircraft Systems  
MS A01-10  
Bethpage, NY 11714-3582

Dr. John Dugan, Jr.  
Cortana Corp.  
520 N. Washington St.  
Falls Church, VA 22046

Mr. William Ferrara  
CASDE Corp.  
2300 Shirlington Rd.  
Suite 600  
Arlington, VA 22206

Dr. Don Flaggs  
Mechanics and Materials Lab  
Org 93-30 B/251  
3251 Hanover St.  
Palo Alto, CA 94304-1191

Dr. Chris Fortunko  
NIST, Mail Code 430  
325 South Broadway  
Boulder, CO 80303

Mr. L.B. Greszczuk  
McDonnell Space Systems Company  
5301 Bolsa Avenue  
Hunington Beach, CA 92647

Ms. Tricia Hankinson  
PRC, Inc.  
1555 Wilson Blvd., Suite 600  
Arlington, VA 22209

Mr. Jeffrey D. Hendrix  
Hercules Aerospace Co.  
1800 K Street NW, Suite 710  
Washington, DC 20006

Ms. Diana Holdinghausen  
McDonnell Aircraft Company  
D357, MC 1021310  
PO Box 516  
St. Louis, MO 63166

Mr. Pete Hoffman  
McDonnell Aircraft Company  
D357, MC 1021310  
PO Box 516  
St. Louis, MO 63166

Dr. Dan King  
McDonnell Aircraft Company  
MC1021310  
PO Box 516  
St. Louis, MO 63166

Mr. Steve Kopf  
EI DuPont DeNemours & Co.  
Composites Div.  
Chestnut Run Plaza  
Box 80702  
Wilmington, DE 19880-0702

Mr. G. Leon  
General Dynamics, EB Div.  
Dept. 442, Station J11-431  
Eastern Pt. Rd.  
Groton, CT 06340

Mr. R. E. Lovejoy  
Coastal Systems Station  
Code 30E  
Panama City, FL 32407-5000

Mr. John MacKay  
Touchstone Research Laboratory  
The Millennium Centre  
Triadelphia, WV 26059

Dr. Ralph Nuismer  
Hercules Composite Structures  
Mail Stop X11K4  
PO Box 98  
Magna, UT 84044-0098

Mr. Jim Suarez  
Grumman Aircraft Systems  
MS B44/35  
Bethpage, NY 11714-3582

Mr. Thomas Triplett  
ICI Composite Structures  
2055 East Technology Circle  
Tempe, AZ 85284

Mr. Charles Zanis  
CASDE Corporation  
2800 Shirlington Road  
Suite 600  
Arlington, VA 22206

Dr. John H. Bode  
Alliant Techsystems  
7225 Northland Drive  
Brooklyn Park, MN 55428

Dr. Reaz Chaudhuri  
Dept. of Civil Eng.  
3220 Merrill Eng. Bldg.  
Univ. of Utah  
Salt Lake City, UT 84112

Dr. Bob Green  
Director, CNDE  
102 Maryland Hall  
The Johns Hopkins Univ.  
Baltimore MD, 21218

Dr. Jeff Hall  
General Dynamics, EB Div.  
Dept. 442, Station J11-431  
Eastern Pt. Rd.  
Groton, CT 06340

Mr. Gregory N. Skaper  
L. J. Broutman & Assoc. Ltd.  
3424 South State St.  
Chicago, IL 60616

Mr. Paul Miller  
Newport News Shipbuilding  
& Drydock Company  
San Diego Office  
1550 Hotel Circle, N.  
Suite 400  
San Diego, CA 92108

Robert Pasternak  
US AMTL  
Attn. SLCMT-MRM  
Watertown, MA 02172-0001

K. A. Stubenhofer  
Information Center  
Lord Corp.  
PO Box 10039  
Erie, PA 16514

Mr. John M. Winter, Jr.  
CNDE  
102 Maryland Hall  
The Johns Hopkins University  
Baltimore, MD 21218

Prof. Michael Wisnom  
Dept. of Aerospace Engineering  
University of Bristol  
Queens Bldg., Univ. Walk  
Bristol, BS8 1TR

Dr. Fuh-Gwo Yuan  
Department of Mechanical  
& Aerospace Engineering  
North Carolina State University  
Raleigh, NC 27695-7910

REPORT DOCUMENTATION PAGE			Form Approved OMB No. 0704-0188	
<small>Public reporting burden for this collection of information is estimated to average 1 hour per response, including the time for reviewing instructions, searching existing data sources, gathering and maintaining the data needed, and completing and reviewing the collection of information. Send comments regarding this burden estimate or any other aspect of this collection of information, including suggestions for reducing this burden, to Washington Headquarters Services, Directorate for Information Operations and Reports, 1215 Jefferson Davis Highway, Suite 1204, Arlington, VA 22202-4302, and to the Office of Management and Budget, Paperwork Reduction Project (0704-0188), Washington, DC 20503.</small>				
1. AGENCY USE ONLY (Leave blank)		2. REPORT DATE April 1992		3. REPORT TYPE AND DATES COVERED RDT&E
4. TITLE AND SUBTITLE (U) KINK-BAND FAILURE ANALYSIS OF THICK COMPOSITES IN COMPRESSION			5. FUNDING NUMBERS Work Unit No. 1-1720-476 & 1-2802-304	
6. AUTHOR(S) E. T. Camponeschi, Jr., J. W. Gillespie, Jr., D. J. Wilkins				
7. PERFORMING ORGANIZATION NAMES(S) AND ADDRESS(ES) David Taylor Research Center Annapolis, MD. 21402-5067 Defense Advanced Research Projects Agency 3701 N. Fairfax Drive Arlington, VA 22217			8. PERFORMING ORGANIZATION REPORT NUMBER CARDEROCKDIV-SME-92/29	
9. SPONSORING / MONITORING AGENCY NAMES(S) AND ADDRESS(ES) David Taylor Research Center, Code 2723 Annapolis, MD. 21402-5067			10. SPONSORING / MONITORING AGENCY REPORT NUMBER	
11. SUPPLEMENTARY NOTES				
12a. DISTRIBUTION / AVAILABILITY STATEMENT Approved for public release; distribution is unlimited.			12b. DISTRIBUTION CODE	
13. ABSTRACT (Maximum 200 words) <p>This paper describes an analysis of 6.4 to 25.4 mm (0.25 to 1.0 in.) thick composite laminates subjected to uniaxial compressive loading that experimentally showed a decrease in strength with increasing thickness. The analysis was performed to determine if the reduction in strength was an intrinsic thickness material effect or if it could be attributed to through-thickness restraint on the specimen caused by the test fixture. The analysis was based on closed form solutions for the formation of kink-band failures in the presence of fibers misaligned with the principal axis of compression loading. The fiber misalignment was determined by a finite element analysis that accounted for the displacement of the laminate outer plies where the laminate exited the compression test fixture. The correlation between the experimental results and the theoretical analysis showed the compression strength of the AS4/3501-6 and S2/3501-6 laminates to be independent of thickness and directly proportional to the through-thickness fixture restraint on through-thickness Poisson expansion. This theoretical and experimental comparison also demonstrated a strong correlation between fiber misalignment, its resulting shear stress state and the kink-band compression failure mechanism.</p>				
14. SUBJECT TERMS Composite Materials, Compression failure, Kink-Bands, Thick Composites			15. NUMBER OF PAGES 28	
			16. PRICE CODE	
17. SECURITY CLASSIFICATION OF REPORT Unclassified	18. SECURITY CLASSIFICATION OF THIS PAGE Unclassified	19. SECURITY CLASSIFICATION OF ABSTRACT Unclassified	20. LIMITATION OF ABSTRACT Same as report	